Assessment of Brain Glucose Metabolism Following Cardiac Arrest by [18F]FDG Positron Emission Tomography

Hannah J. Zhang, PhD[1], Samuel Mitchell, BS[1], Yong-Hu Fang, MD[2], Hsiu-Ming Tsai, PhD[3], Lin Piao, PhD[2], Alaa Ousta, MD[2], Lara Leoni, PhD [3], Chin-Tu Chen, PhD[1], Willard W. Sharp, PhD, MD[2]

1. Department of Radiology, University of Chicago, 5814 S Maryland Avenue, Chicago, IL 60637
2. Department of Medicine, Section of Emergency Medicine, University of Chicago, 5841 S Maryland Avenue, Chicago, IL 60637
3. Office of Shared Research Facilities, University of Chicago, 5814 S Maryland Avenue, Chicago, IL 60637

Corresponding author Willard W. Sharp PhD, MD; Department of Medicine, Section of Emergency Medicine, University of Chicago, 5841 S Maryland Avenue, Chicago, IL 60637

Key words Cardiac Arrest; Resuscitation; Brain glucose metabolism; [^{18}F]FDG; Positron emission tomography (PET); Cerebral injury

Abstract

Background Cardiopulmonary resuscitation (CPR) following cardiac arrest (CA) can lead to neurological deficits ranging from minor cognitive impairments to persistent vegetative state and brain death. The pathophysiology of the resulting brain injury is poorly understood and whether changes in post-CA brain metabolism contribute to the injury are unknown. Here we utilized [^{18}F]FDG-PET to study *in vivo* cerebral glucose metabolism 72 hours following cardiac arrest in a murine cardiac arrest model.

Methods Anesthetized and ventilated adult C57BL/6 mice underwent 12-minute KCl-induced CA followed by CPR. Seventy-two hours following cardiac arrest, surviving mice were intraperitoneally injected with [^{18}F]FDG (~186 µCi/200 µl) and imaged on Molecubes preclinical micro PET/CT imaging systems after a 30-minute awake uptake period. Brain [^{18}F]FDG uptake was determined by the VivoQuant software on fused PET/CT images with the 3D brain atlas. Upon completion of PET imaging, remaining [^{18}F]FDG radioactivity in the brain, heart, and liver was determined using a gamma counter.

Results Global increases in brain [^{18}F]FDG uptake in post-CA mice were observed compared to shams and controls. The standardized uptake value (SUV) of [^{18}F]FDG for CA animals was 1.93±0.28 vs. sham 1.19±0.09 ($p<0.05$) and control animals 0.61±0.31 ($p<0.01$). This increased uptake was consistent throughout the 60-minute imaging period and across all brain regions reaching statistical significance in the midbrain, cerebellum, medulla, pons, and thalamus. Biodistribution analyses of various key organs yielded similar observations as for brain [^{18}F]FDG uptake (6.82±0.61%ID/g tissue for CA mice vs 4.90±0.55%ID/g tissue for sham animals, $p<0.05$).

Conclusions This study is the first successful application of using PET/CT imaging to measure changes in brain metabolism, utilizing brain [^{18}F]FDG uptake, in a murine model of asystolic CA. Our results demonstrate increased [^{18}F]FDG uptake in the brain 72 hours following CA, suggesting increased

metabolic demand in the case of severe neurological injury. Further study is warranted to determine the etiology of these changes.

Introduction

Each year there are approximately 550,000 cardiac arrests (CA) both in and out of the hospital each year in the United States[1]. Despite improvements in cardiopulmonary resuscitation, morbidity and mortality in successfully resuscitated patients is high[2,3]. Although multi-organ injury is not uncommon, many post-CA patients die primarily in the context of severe hypoxic encephalopathy[4]. Currently post-cardiac arrest hypothermia and supportive care are the only treatments for managing post-CA neurological injury. The pathology of post-cardiac arrest neurological injury is not well understood and there are few studies investigating change in brain metabolism following post-CA resuscitation.

As a glucose analogue, [^{18}F]fluorodeoxyglucose ([^{18}F]FDG) is an FDA approved positron emission tomography (PET) radiotracer, routinely used in the clinical prognosis and diagnosis of cancer and the determination of overall tissue metabolic demand. Similar to glucose metabolism, once [^{18}F]FDG is transported into cells by glucose transporters, it is irreversibly phosphorylated and trapped intracellularly. However, in contrast to glucose, [^{18}F]FDG does not undergo further glycolysis due to its lack of a 2-hydroxyl group. Therefore, [^{18}F]FDG is not only used in tumor imaging, but is also utilized to evaluate the function of tissues with high glycolytic rates including brains. To date, there have been only a few pre-clinical investigations examining post-cardiac arrest brain metabolism using [^{18}F]FDG-PET in dogs and rats in the first several hours following resuscitation[5,6]. However, neither of these studies examined time points distant from the cardiac arrest when post-CA brain injury is likely to be evolving and neither of these studies reported the neurological outcomes of the animals studied. In this study we overcome these limitations by assessing global and regional changes in brain glucose metabolism 72 hours following cardiac arrest using [^{18}F]FDG-PET in a mouse model and report how these changes relate to the neurological outcomes in the animals studied.

Material and Methods

Animals

Mature female C57BL/6 mice (3.63±0.04 months) were used in the experiments. Animals were housed in The University of Chicago Animal Research Resources Center. The Institutional Animal Care and Use Committee of the University of Chicago, in accordance with National Institutes of Health guidelines, approved all animal procedures. Animals were maintained at 22–24°C on a 12:12-h light-dark cycle and provided food (standard mouse chow) and water ad libitum.

Animal Models of Cardiac Arrest

A modified version of our previously published murine model of asystolic CA was used[7,8]. Briefly, Mice were anesthetized with 3% isoflurane and vascular access was acquired. Temperature, respirations, and EKG tracings were recorded continuously on a PowerLab data acquisition module (AD Instruments, Colorado Springs, CO). A 0.4 mm OD heparinized micro PE cannula (BioTime Inc., Berkeley, CA) was placed in the left jugular vein for fluid administration and right carotid artery for aortic systolic pressure (ASP) measurement. Asystolic CA was induced with a single bolus of KCl (0.8 mg/g body weight) into the internal jugular vein and ventilation was suspended. Following 12 min of CA, cardiopulmonary resuscitation (CPR) was performed at approximately 300-350 beats/min. After 90 seconds of CPR, 1.5 µg of epinephrine was injected followed by a saline flush. CPR was terminated when return of spontaneous circulation (ROSC), defined by a mean arterial pressure >40 mm Hg lasting longer than 5 minutes, was achieved. CPR was terminated if ROSC was not achieved after 5 minutes. Quality of CPR was retrospectively evaluated for each animal by reviewing CPR rates and arterial pressures. Resuscitated animals received IV 0.9% saline at a rate of 100 µl/hr and were monitored on mechanical ventilation for 120 minutes. Thereafter, the mice were extubated and allowed free access to food and water. Sham animals underwent similar operations as the CA animal without induction of CA. Control animals did not undergo any surgery. The mice were observed every 2 hours during the first 6 hours following CA. Animals were then returned to the animal facility.

Neurological Scoring

Neurological score of mice after CA (2h, 6h, 24h, 48h and 72h) were determined using a 12-point mouse neurological scoring system[7]. Scores ranged from 0 (no response or worst) to 2 (normal) along 6 domains: paw pinch, righting reflex, breathing, spontaneous movement, motor-global and motor-focal. The scores for each of the 6 domains were determined in a blinded fashion and summed to calculate the neurological score.

[^{18}F]FDG Imaging

Control animals (n=3) were imaged without any surgery or treatment. Other animal were imaged 72 hours post-surgery. Following an overnight fast, all mice (22.6±0.8 g) received 186±3 μCi of [^{18}F]FDG (Sofie Biosciences Inc, Dulles, VA) intraperitoneally in 200 μl, diluted in isotonic saline solution. After a 30-minute uptake awake period, total body PET imaging was acquired on the β-cube preclinical microPET imaging system (Molecubes, Gent, Belgium) for one hour. A reference CT image was then acquired on the X-cube preclinical microCT imaging system, (Molecubes, Gent, Belgium). Dynamic PET reconstruction was set-up with six 10-munite frames using an OSEM reconstruction algorithm. Images were reconstructed with 400 μm isotropic voxel size. CT images were reconstructed with a 200 μm isotropic voxel size and used for anatomic co-registration and scatter correction. Animals were maintained under 1-2% isoflurane anesthesia in oxygen during imaging. Respiration and temperature were constantly monitored using the Molecubes monitoring interface, as well as Small Animal Instruments (SAII Inc, Stoney Brook, NY) set up. All of the animals survived the imaging.

Data Analyses of [^{18}F]FDG Uptake

To quantify brain [^{18}F]FDG uptake, analyses of CT-fused PET images were performed using VivoQuant software (Invicro, Boston, MA). Dynamic [^{18}F]FDG uptake was obtained and expressed in standardized uptake value (SUV) for the six 10-minute frames. Brain regions of interest (ROI) were segmented using the 3D brain atlas within the VivoQuant software. The regional absolute [^{18}F]FDG

uptake was obtained. And percentage differences of [^{18}F]FDG uptake between the CA and the sham for each individual region were calculated using the mean uptake of the each group. [^{18}F]FDG uptake of the heart and the liver was done similarly by drawing the ROI of the heart and liver respectively with CT guided anatomy. To normalize the uptake variation from each individual animal, liver was used as reference region for the uptake of brain. The fold change between the brain and the liver was expressed as the relative [^{18}F]FDG uptake.

Biodistribution of [^{18}F]FDG

Biodistribution of [^{18}F]FDG uptake was performed after the PET/CT imaging. The brains, hearts, and livers were isolated and weighed. Radioactivity of the organs was measured on a Cobra II gamma counter (PerkinElmer, Waltham, MA). The normalized percentage of uptake (%ID/g tissue) was calculated by dividing the decay-corrected activity in an organ to the total injected dose and normalizing to the weight of the organ.

Statistical Analyses

Statistical analyses were performed using Prism software (GraphPad, La Jolla, CA, USA). The survival rate between sham and CA animals was evaluated by the Log-rank (Mantel-Cox) test. Continuous data were summarized as means ± SEM, with statistically significant differences assessed using an unpaired Student's *t*-test between 2 groups and one-way ANOVA between multiple groups. The differences of neurological scores between sham and CA groups were determined by two-way ANOVA using the Bonferroni post hoc test. The correlation analyses were done using simple linear regression. $p<0.05$ was considered statistically significant.

Results

In this study, age and weight matched (Figure 1B) mice were randomly divided into sham and CA groups on the day of surgery. Animals underwent similar surgery procedures as outlined in the scheme

of Figure 1A, except that CA was not induced in sham animals. Seventy-two hours after the surgery, only 64% of the CA mice (9 out of 14) survived, compared to 100% survival from the sham animals (8 out of 8). However, among those that survived, CA mice showed neurological disability as early as 2 hours after resuscitation. By 72 hours, the neurological scores in CA mice had improved compared with the scores at 2 hours post CA, but were still significantly lower than those of sham mice ($P<0.05$, Figure 1C).

Figure 2A shows the [^{18}F]FDG uptake of 5 representative coronal sections from anterior to posterior portion of the brain in sham (bottom) and CA (top) mice. The image at the bottom of coronal sections is a schematic diagram of sagittal view of the brain with 5 perpendicular lines showing approximately position where the coronal sections were taken. The [^{18}F]FDG uptake was consistent over the 1 hour period of the imaging as analyzed by the dynamic reconstruction (data not shown). Therefore, the averaged SUVs from those of six 10-min time frames were used for the comparison of [^{18}F]FDG uptake among control, sham and CA mice. On average, the global brain [^{18}F]FDG uptake was significantly higher in CA mice than that in the sham animals, $p<0.05$ and controls, $p<0.01$ (Fig 2B). The [^{18}F]FDG uptake of liver and heart was also measured simultaneously but no differences were found (Fig 2D & 2F). These observations were confirmed by the ex-vivo biodistribution analyses measuring the radioactivity of individual organs isolated after the imaging (Fig 2C, 2E, &2G).

To further investigate whether the cerebral [^{18}F]FDG uptake was related to the neurological injuries, the correlation between the neurological scores and the SUV was analyzed by simple linear regression method (Figure 3). An inverse relationship, showing the lower neurological score the higher brain SUV, was found with a statistically significant correlation at the 24 hour ($r^2=0.2722$, $p=0.0461$) (Figure 3A) and 48 hour ($r^2=0.2972$, $p=0.0356$) (Figure 3B) post-CA, demonstrating . A trend of inverse correlation was also found for the time points of 2 hours ($r^2=0.0945$, $p=0.2467$) (Figure 3C), 6 hours ($r^2=0.1926$, $p=0.1018$) (Figure 3D), and 72 hours ($r^2=0.1968$, $p=0.0977$) (Figure 3E) after the

CA, but statistical significance was not achieved for these time points.

The brain was further divided into 14 regions using 3D atlas available with the VivoQuant software. Figure 4C shows the representative coronal, transverse, and sagittal sections (left, middle, and right) of a CA mouse brain that are over laid with the 3D atlas. Absolute [^{18}F]FDG uptake of all 14 regions are presented in Figure 4A. Overall, the lowest uptake was seen in the cortex with a mean SUV 1.03 for the sham group and 1.67 for the CA group. The medulla region had the highest [^{18}F]FDG uptake with mean SUV value at 1.41 for sham mice and 2.30 for CA mice. Compared to shams, all 14 brain regions showed increased absolute [^{18}F]FDG uptake in post-CA animals with statically significance in 8 out of 14 regions ($p<0.05$) involving the midbrain, pons, medulla, cerebellum, thalamus, corpus callosum, ventricles, and olfactory (Fig 4A). The percentage mean differences between sham and CA group were calculated for all 14 regions (Figure 4B). Midbrain has the largest difference (43.2%) while pallidum has the smallest difference (34.1%).

Whole brain and regional relative [^{18}F]FDG uptake after the brain uptake was normalized to the liver uptake for each individual animal is shown in Figure 5. Similar to the absolute SUV, the global cerebral [^{18}F]FDG uptake was significantly higher in CA mice than the shams ($p<0.05$) (Figure 5A), while 5 (midbrain, pons, cerebellum, medulla, and thalamus) out of 14 regions showed significantly elevated[^{18}F]FDG uptake ($p<0.05$) (Figure 5B).

Discussion

According to a 2015 American Heart Association report, only 8.3% of those who survived the cardiac arrest return to their former quality of life[9]. The majority of the cardiac survivors sustain certain degrees of neurological injuries ranging from mild cognitive defects, impaired consciousness, to more serious conditions such as remaining in a persistent vegetation state. To date, the only therapies for this injury is conservative intensive care unit care and therapeutic hypothermia. And outcomes are highly

variable.

The brain consumes 25% of total body glucose as its primary source of energy[10,11], even though it only makes up 2% of total body weight. Therefore, quantification of glucose metabolism may be a good indicator of overall brain function. Using the clinically available PET tracer, [^{18}F]FDG, we examined changes in brain glucose metabolism in response to post-CA resuscitation. Surviving post-CA mice had evidence of neurological injury as reflected by their neurological scores (Fig 1C). In contrast to our expectations of observing decreased brain metabolism in post-CA mice, we observed increases in brain glucose uptake in 72 hours post-CA animals.

Currently, prognosis of cardiac arrest patients is mainly dictated by the distribution and degree of cerebral ischemic injury[12]. Much of the research focuses primarily on changes in cerebral blood flow or neuroanatomy. No functional measurement is clinically available at this point. For the first time, we established a correlation between cerebral glucose metabolism and CA induced neurological injury using [^{18}F]FDG-PET imaging. When assessing differences of [^{18}F]FDG uptake within specific brain regions, statistically significant elevations were found in 8 out of 14 regions analyzed. Clinically, cerebellum, thalamus, corpus striatum, and hippocampus are known to be vulnerable to CA induced injuries[13]. In particular, imaging studies using diffusion-weighted magnetic resonance (MRI) consistently report reduced diffusion within the *cornu Ammon* neurons of the hippocampus, cerebellar Purkinje cells, and cerebral cortex [14-17]. The finding in this study correlates with clinical outcomes in human patients for CA. Therefore, [^{18}F]FDG-PET may have clinical significance, providing a non-invasive approach for the diagnostic and therapeutic strategies in the treatments post CA.

After normalizing individual variations using liver [^{18}F]FDG uptake as reference, the regions consisting of brainstem (midbrain, pons, and medulla) and its adjacent area (cerebellum and thalamus) presented the largest and statistically significant increase of glucose uptake. Brainstem controls basic body functions and is a crucial part transporting signals between brain and the body. In 2010, Xu et al.

reported a suppressed brainstem mitochondrial respiratory rate four days following cardiac arrest and resuscitation in aged rats[18]. It is thus indicative that our results in this study reflect a switch of glucose metabolism from oxidative respiration to increased glycolysis. Further experiments to test this idea are ongoing.

In two previous pre-clinical studies using piglet and rat models of cardiac arrest, lowered cerebral uptake of [^{18}F]FDG 2 to 48 hours after CA were observed[5,6]. In contrast, our study demonstrated statistically significant 1.6 and 3.2 fold increases of whole brain [^{18}F]FDG uptake in CA mice compared to sham and control mice respectively (SUV 1.93 vs 1.19 and 1.93 vs 0.62) 72 hours after CA. Our study differed from these previous studies in several important aspects which may explain the differences in our findings. First, our study performed neurological assessments of sham and post-CA animas which the prior studies lacked. We found that our observed changes in brain metabolism correlated with the severity of neurological outcomes of the mice. Second, our study used a longer cardiac arrest duration (12 min vs 6-8 min), possibly resulting in more severe injury. Third our [^{18}F]FDG-PET imaging was done much later following cardiac arrest (72 hours vs 2-48 hours) and possibly reflects progressing late brain injury which often does not become apparent until days following cardiac arrest. Importantly, Putzu et al. showed increased relative brain [^{18}F]FDG uptake in several rat brain regions (midbrain, pons, medulla, and cerebellum), which are similar to our regional analyses, despite a conclusion of lowered cerebral [^{18}F]FDG uptake[5].

The etiology of the increased metabolic demand as reflected by increased glucose utilization following cardiac arrest despite the depressed neurological state of these animals is uncertain. Possible explanations for these observations include increased neuro excitotoxicity stimulated by the ischemia-reperfusion injury or alternatively due to post-cardiac arrest inflammatory changes occurring in the brain. Further studies are needed to investigate these possibilities.

Conclusions

Asystolic cardiac arrest induced increases in global brain glucose uptake 72 hours following resuscitation. The degree of the increase corresponded to the neurological injury observed in these animals. When compared to the shams, elevated glucose uptake in post-CA mice was particularly significant in the brainstem and adjacent regions. Increased glucose uptake in these brain regions could be reflective of metabolic shifts or of post-CA inflammatory changes in these regions. Further study of the mechanisms underlying these observations is warranted.

Acknowledgements The authors acknowledge the assistance from the Intergrative Small Animal Imaging Research Resources (ISAIRR) of the University of Chicago supported in part by the NIH grant P30 CA14500. The authors thank Nathanial Holderman and Andrew McVea for technical support.

Funding The study was supported in part by the NIH grant 1UL1TR002389-01 to the Institute for Translational Medicine (ITM) of the University of Chicago, by the NIH grant RO1HL133675 to WWS, and by the NIH training grant T32HL007381 to AO.

References

1. Benjamin EJ, Virani SS, Callaway CW, et al. Heart Disease and Stroke Statistics-2018 Update: A Report From the American Heart Association. Circulation 2018;137:e67-e492.
2. Wu O, Sorensen AG, Benner T, Singhal AB, Furie KL, Greer DM. Comatose patients with cardiac arrest: predicting clinical outcome with diffusion-weighted MR imaging. Radiology 2009;252:173-81.
3. Järnum H, Knutsson L, Rundgren M, et al. Diffusion and perfusion MRI of the brain in comatose patients treated with mild hypothermia after cardiac arrest: a prospective observational study. Resuscitation 2009;80:425-30.
4. Witten L, Gardner R, Holmberg MJ, et al. Reasons for death in patients successfully resuscitated from out-of-hospital and in-hospital cardiac arrest. Resuscitation 2019;136:93-9.
5. Putzu A, Valtorta S, Di Grigoli G, et al. Regional Differences in Cerebral Glucose Metabolism After Cardiac Arrest and Resuscitation in Rats Using [Neurocrit Care 2018;28:370-8.
6. Li YQ, Liao XX, Lu JH, et al. Assessing the early changes of cerebral glucose metabolism via dynamic (18)FDG-PET/CT during cardiac arrest. Metab Brain Dis 2015;30:969-77.
7. Zhao D, Abella BS, Beiser DG, et al. Intra-arrest cooling with delayed reperfusion yields higher survival than earlier normothermic resuscitation in a mouse model of cardiac arrest. Resuscitation 2008;77:242-9.
8. Sharp WW, Beiser DG, Fang YH, et al. Inhibition of the mitochondrial fission protein dynamin-related protein 1 improves survival in a murine cardiac arrest model. Crit Care Med 2015;43:e38-47.
9. Kavi T, Desai M, Yilmaz FM, Kakadia B, Burakgazi-Dalkilic E, Shrestha GS. Inter-predictability of Neuroprognostic Modalities After Cardiac Arrest. Cureus 2019;11:e4489.

10. Dienel GA. Brain Glucose Metabolism: Integration of Energetics with Function. Physiol Rev 2019;99:949-1045.
11. Zauner A, Muizelaar JP. Brain metabolism and cerebral blood flow. In: Reilly P, Bullock R, eds. Head Injury. First ed. London: Chapman & Hall; 1997:89-99.
12. Madl C, Holzer M. Brain function after resuscitation from cardiac arrest. Curr Opin Crit Care 2004;10:213-7.
13. Wijdicks EF, Campeau NG, Miller GM. MR imaging in comatose survivors of cardiac resuscitation. AJNR Am J Neuroradiol 2001;22:1561-5.
14. Paine MG, Che D, Li L, Neumar RW. Cerebellar Purkinje cell neurodegeneration after cardiac arrest: effect of therapeutic hypothermia. Resuscitation 2012;83:1511-6.
15. Wijman CA, Mlynash M, Caulfield AF, et al. Prognostic value of brain diffusion-weighted imaging after cardiac arrest. Ann Neurol 2009;65:394-402.
16. Cui D, Shang H, Zhang X, Jiang W, Jia X. Cardiac arrest triggers hippocampal neuronal death through autophagic and apoptotic pathways. Sci Rep 2016;6:27642.
17. Shoykhet M, Simons DJ, Alexander H, Hosler C, Kochanek PM, Clark RS. Thalamocortical dysfunction and thalamic injury after asphyxial cardiac arrest in developing rats. J Neurosci 2012;32:4972-81.
18. Xu K, Puchowicz MA, Sun X, LaManna JC. Decreased brainstem function following cardiac arrest and resuscitation in aged rat. Brain Res 2010;1328:181-9.

Figure legends

Figure 1. Cardiac arrest induces sustained neuronal damage in resuscitated mice. A) A study time line of animals underwent cardiac arrest (CA) induction and sham treatment. Control animals did not undergo any surgery. B) Table showing animal baseline characteristics and post cardiac arrest survival. C) Neurological outcome was evaluated according to six preset scoring criteria at 2, 6, 24, 48, and 72 hours following CA/resuscitation. CA animals had a significantly lower average score suggesting an increased neurological damage.

Figure 2. Cardiac arrest increases global brain [^{18}F]FDG uptake in mice 72 hours post resuscitation. A) Representative coronal sections from anterior to posterior portions of [^{18}F]FDG-PET/CT brain imaging for CA and sham mice. B) Quantification of whole brain [^{18}F]FDG uptake as measured by standardized uptake value (SUV) demonstrates a 1.6 and 3.2 fold higher uptake in CA animals vs. sham ($p<0.05$) and control mice ($p<0.01$) respectively. C) Ex-vivo average whole brain [^{18}F]FDG activity of CA and sham mice as measured by the biodistribution (6.8 vs 4.9%ID/g tissue, $p<0.05$). D) & E) Quantification of liver and heart [^{18}F]FDG uptake as measured by standardized uptake value (SUV). No differences between groups were found. F) & G) Ex-vivo liver and heart [^{18}F]FDG activity of CA and sham mice as measured by the biodistribution. No differences between groups were found.

Figure 3. The increase in brain [^{18}F]FDG uptake correlates with neurological injury induced by CA. Linear regression correlations between the whole brain SUV at 72 hour post CA and neuro scores at different time points post CA were plotted. Inverse relationships were found for all the plots. A) & B) The statistically significance was found between whole brain [^{18}F]FDG uptake and neurological score measured at 24 and 48 hr post-CA. C), D) & E) No statistical significance was observed despite a trend of inverse relationship is evident.

Figure 4. Regional analyses of the brain [^{18}F]FDG uptakes. A) Absolute [^{18}F]FDG uptake for 14 functional brain regions segmented using a 3D atlas. Eight of 14 regions showed a significant increase in [^{18}F]FDG uptake in CA mice compared to sham mice. B) Percentage differences of the mean SUV between CA and sham animals. C) Representative coronal, transverse and sagittal sections of brain images that are overlaid with the 3D atlas.

Figure 5. Relative brain [^{18}F]FDG uptakes normalized to that of liver. A) Whole brain relative [^{18}F]FDG uptake. B) Regional relative [^{18}F]FDG uptakes.

Figure 1. Cardiac arrest induces sustained neuronal damage in resuscitated mice.

A.

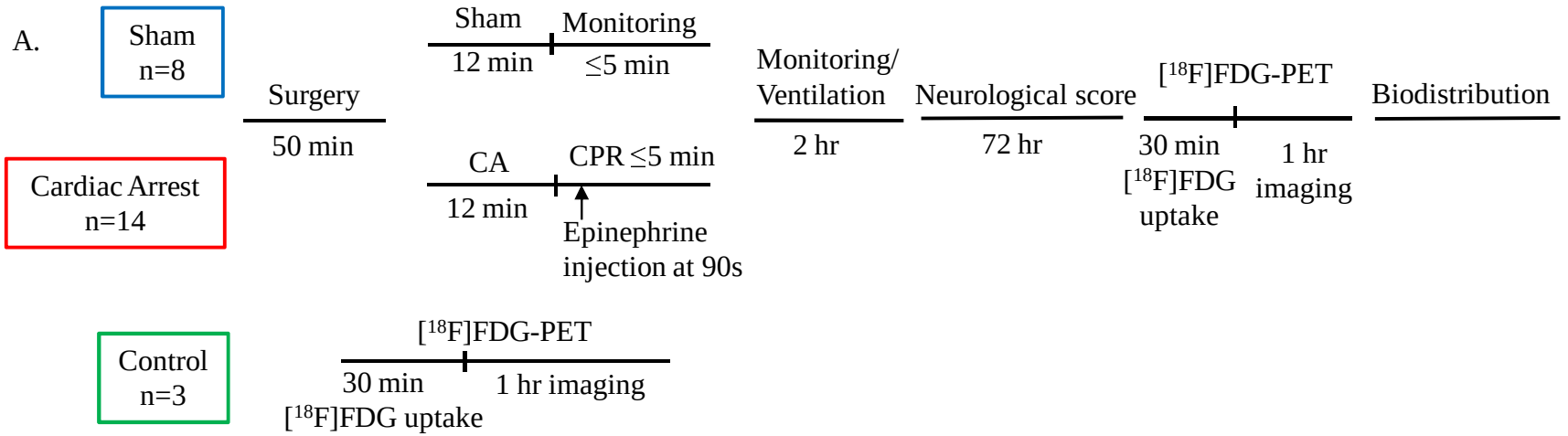

B.

	Sham	CA	P value
Survived/total	N=8/8	N=9/14	
Survival rate	100%	64%	0.006
Age (month)	3.60±0.05	3.64±0.05	0.55
Body weight (g)	22.9 ± 1.2	22.3 ±1.2	0.76
[18F]FDG dose (μCi)	187 ± 5	186 ± 5	0.91

C.

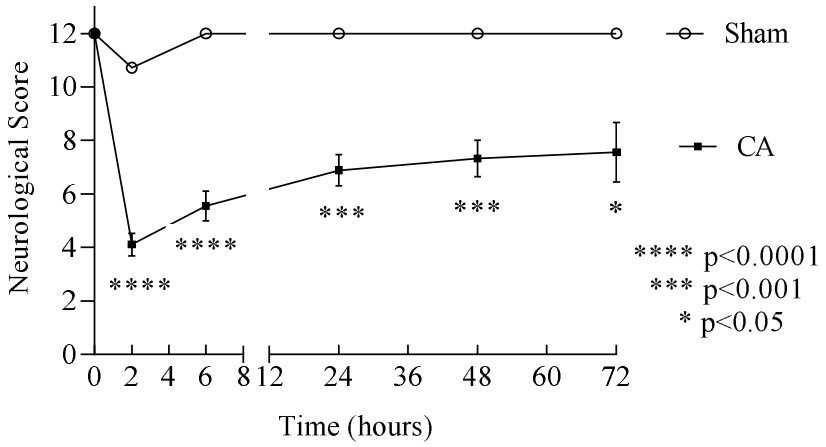

Figure 2. Cardiac arrest increases global brain [^{18}F]FDG uptake in mice 72 hours post resuscitation.

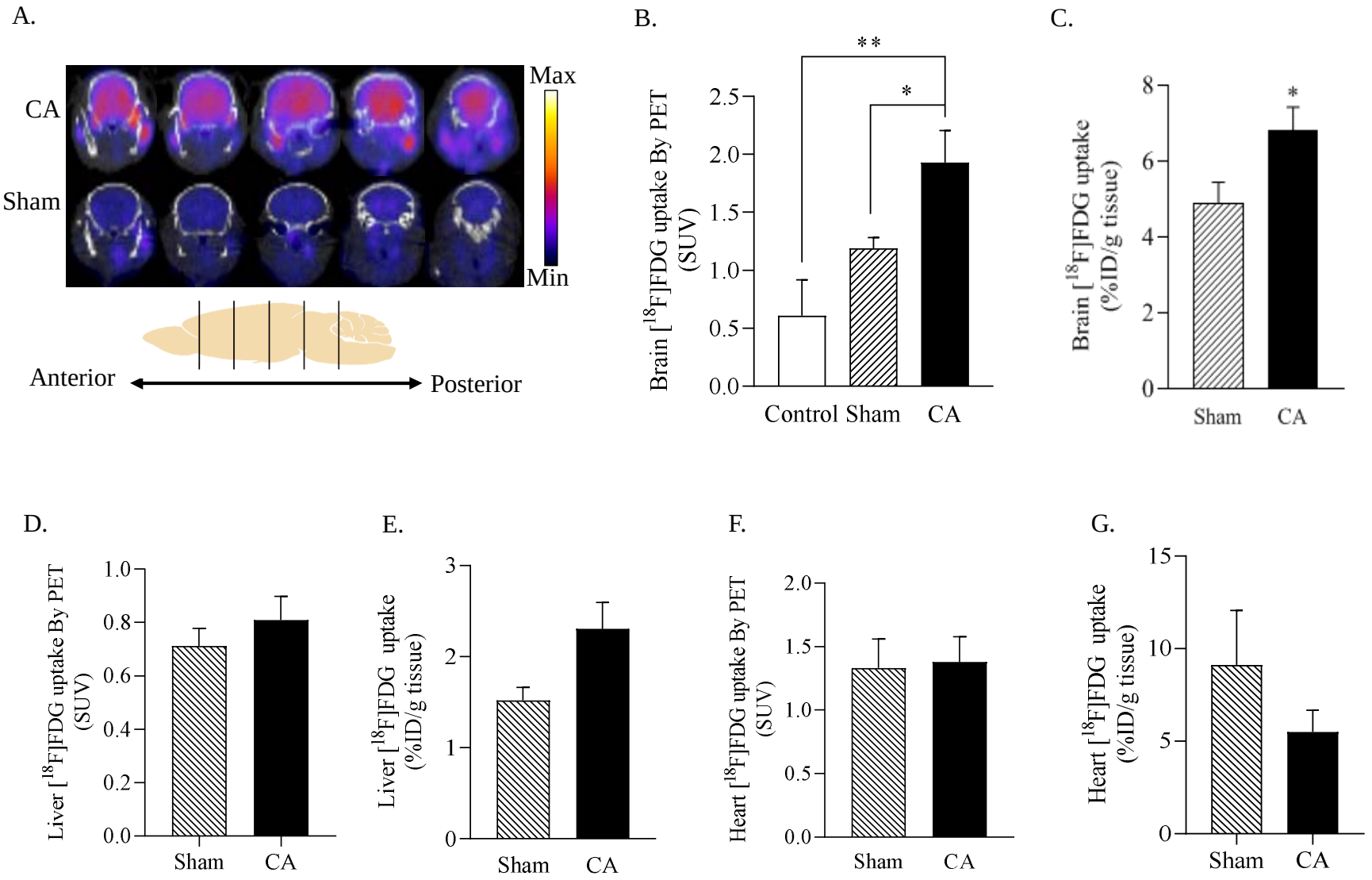

Figure 3. The increase of brain [^{18}F]FDG uptake correlates with neurological injury induced by CA.

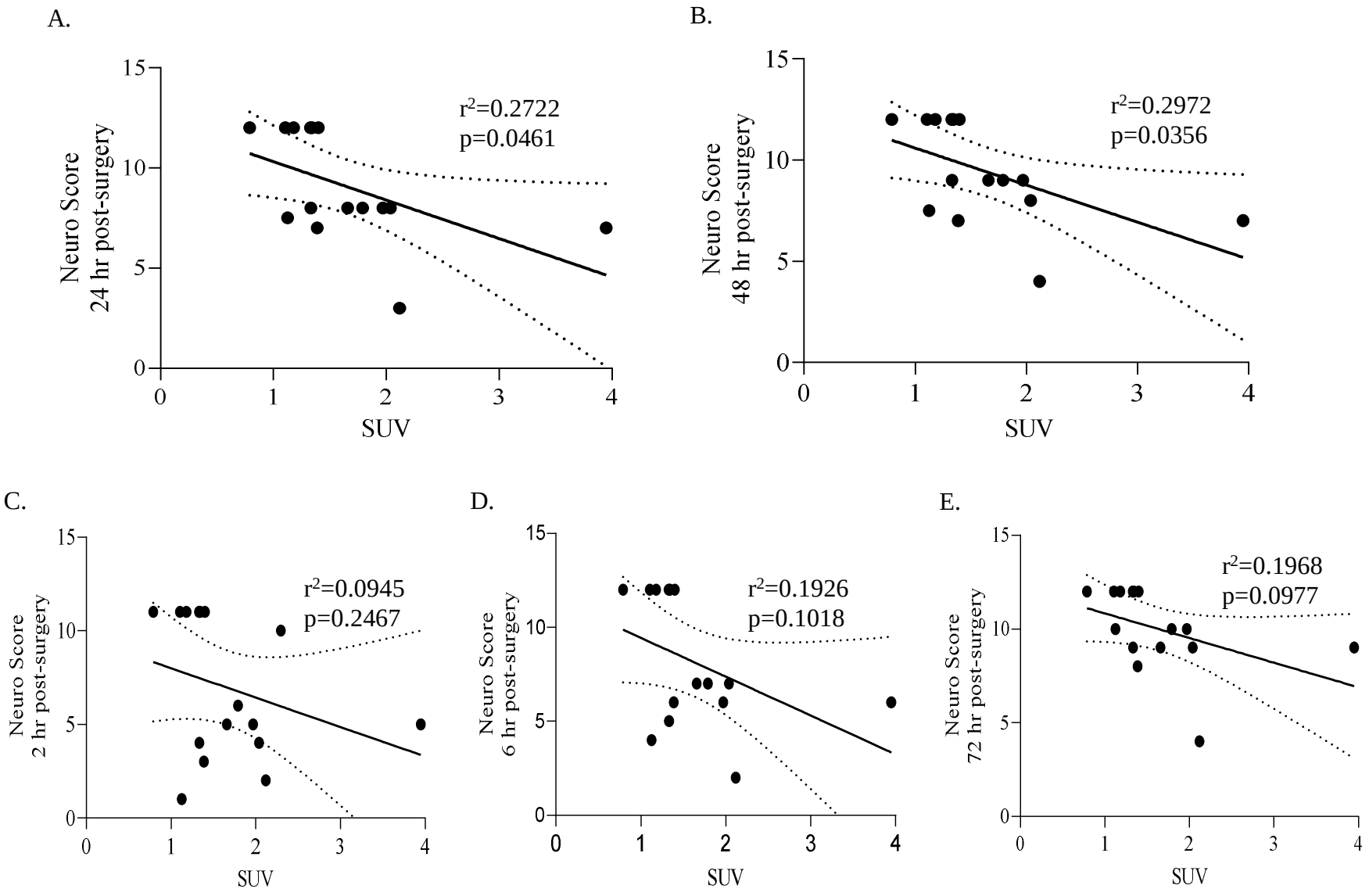

Figure 4. Regional analyses of the brain [^{18}F]FDG uptakes.

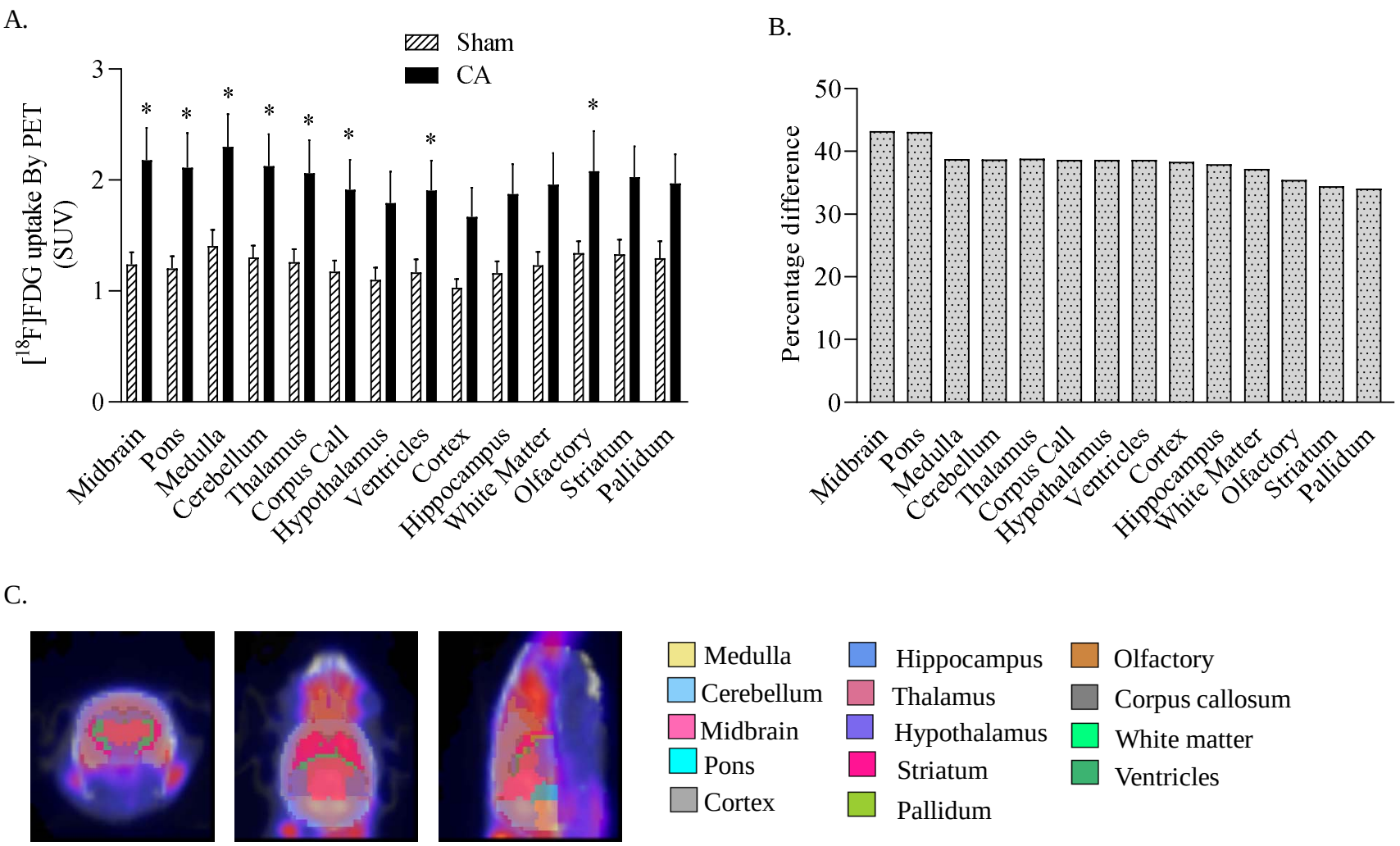

Figure 5. Relative brain [^{18}F]FDG uptakes normalized to that of liver.